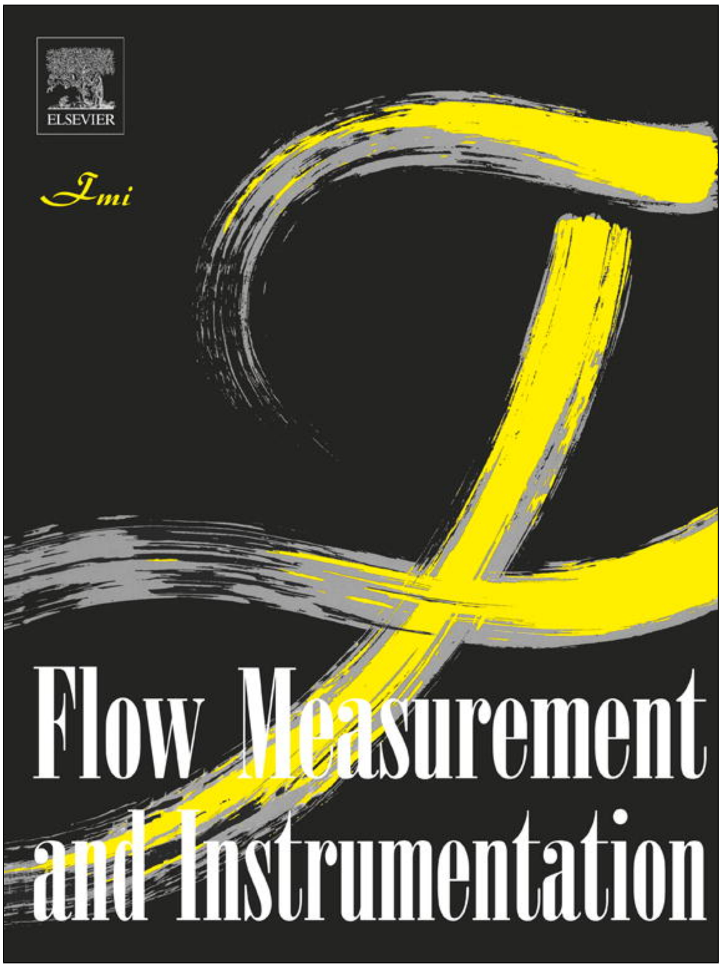

(This is a sample cover image for this issue. The actual cover is not yet available at this time.)

Flow Measurement and Instrumentation 29 (2013) 45–51

Contents lists available at SciVerse ScienceDirect

Flow Measurement and Instrumentation

journal homepage: www.elsevier.com/locate/flowmeasinst

Study of flow at side weir in narrow flume using visualization techniques

Gorazd Novak [a,*], Daniel Kozelj [a], Franc Steinman [a], Tom Bajcar [b]

[a] University of Ljubljana, Faculty of Civil and Geodetic Engineering, Chair of Fluid Mechanics with Laboratory, Hajdrihova 28, Ljubljana, Slovenia
[b] University of Ljubljana, Faculty of Mechanical Engineering, Aškerčeva 6, Ljubljana, Slovenia

ARTICLE INFO

Article history:
Received 13 March 2012
Received in revised form
28 September 2012
Accepted 8 October 2012
Available online 23 October 2012

Keywords:
Side weir
Visualization
Velocity field
Discharge coefficient
Dimension analysis
Hydraulic model

ABSTRACT

The purpose of the research was to quantify characteristics of a subcritical flow at a rectangular sharp-crested side weir in a rectangular main channel using non-invasive measuring techniques based on the visualization of the flow. Experiments were carried out in physical models, including nine different dimensions of the side weir and nine combinations of the inflow and tailwater level for each weir, amounting to 81 test runs. Velocity vector fields were measured in various horizontal planes along the side weir using a high speed digital camera and electrolysis-induced hydrogen bubbles as flow tracers. Recorded films were converted into sequences of images which were used for numerical calculation of local velocities. Components of velocity vectors were determined with great spatial and time resolution. Longitudinal profiles of water surface elevation at each side weir were determined using photos of laser-induced vertical section planes. Measured discharges and flow depths were used to formulate new equation for the side weir discharge coefficient using dimensional analysis. The principal results indicated that velocity distribution along the side weir was distinctly non-uniform, with various velocity ratios increasing along the crest. However, the calculated energy grade line was parallel to the main channel bed, indicating that only friction losses were present. The proposed equations for the side weir discharge coefficient gave results that were in good accordance with two other studies.

1. Introduction

Side weirs are hydraulic structures for diverting discharge from a main channel to a lateral channel or a flood plain. They are widely used in irrigation, sewer, wastewater treatment and flood management systems. Flow over side weir is a case of spatially-varied flow with decreasing discharge and can be described with two alternative approaches, *i.e.* energy or momentum approach, which differ in assumptions concerning values of velocity distribution coefficients α (*i.e.* kinetic energy correction coefficient), and β (momentum correction coefficient). Assuming constant specific energy across the weir and constant and uniform velocity distribution across the channel, Rosier [1] gives the general equation of the discharge q per unit length over the weir as:

$$q = 2/3C_d(2g)^{1/2}(h-p)^{3/2} \tag{1}$$

The performance of side weirs was investigated from the pioneering work of De Marchi [2], seminal work of Hager [3], to recent work of Emiroglu et al. [4]. Recent works based on the constant energy approach are by Singh et al. [5], Swamee et al. [6], or Borghei et al. [7]. The effect of specific energy variation was considered by Yüksel [8] and Venutelli [9]. Representative works based on the momentum approach are by El-Khashab and Smith [10], Hager and Volkart [11], Lee and Holley [12] or May et al. [13].

The objectives of the present study were: (1) to quantify vector velocity fields using non-invasive visualization method and thus avoid flow perturbations caused by intrusive instrumentation, (2) to determine longitudinal water surface profile along the side weir using another non-contact visualization technique, and (3) to formulate a new equation for the discharge coefficient C_d using dimensional analysis, *i.e.* Buckingham Π theorem, which allows C_d to be expressed as a product of selected dimensionless ratios of various experimentally measured values. The present study is a continuation of research by Novak et al. [14]. Notations and a definition sketch of investigated side weirs are shown in Fig. 1:

In Fig. 1**a** L_z and z_z represent the sharp-crested rectangular weir for tailwater regulation. Fig. 1**b** shows velocities at cross section x.

2. Material and methods

The goals of this study were reached using mostly experimental setup described by Novak et al. [14] and a visualization

* Corresponding author. Tel.: +386 14253460; mob.: +386 31549134; fax: +386 14269163.
E-mail addresses: gorazd.novak@fgg.uni-lj.si (G. Novak), daniel.kozelj@fgg.uni-lj.si (D. Kozelj), franci.steinman@fgg.uni-lj.si (F. Steinman), tom.bajcar@fs.uni-lj.si (T. Bajcar).

0955-5986/$ - see front matter
http://dx.doi.org/10.1016/j.flowmeasinst.2012.10.008

Nomenclature

Symbols

B	width of the main channel [m]
h	flow depth in the centerline of the main channel [m]
Fr	Froude number
L	length of the side weir crest [m]
p	height of the side weir crest [m]
Q	discharge [m^3/s]
S_0	main channel bed slope [-]
u	velocity component in x direction [m/s]
$\bar{u}$	average velocity in x direction [m/s]
$u_c*(Q)$	uncertainty of flow measurement [%] (notation in accordance with ISO 1438:2008)
$u_c*(\bar{u})$	uncertainty of velocity measurement [%](notation in accordance with ISO 1438:2008)
v	velocity component in transverse direction [m/s]
x	longitudinal direction, also distance from upstream end of the side weir [m]
α	kinetic energy correction coefficient [-]
β	momentum correction coefficient [-]

Indices

1	upstream end of the side weir
2	downstream end of the side weir
s	side weir
w	wire (in connection with electrolysis-induced hydrogen bubbles)
z	weir for regulation of tailwater level

method introduced by Bajcar et al. [15]. In our previous study (Novak et al. [14]) results for velocity ratios $u_s/\bar{u}$, and coefficients α and β from 18 test runs were presented, covering 3 combinations of inflow Q_1 and tailwater weir z_z for each of the 6 side weirs (various crest length L and crest height p) in the $B=14$ cm wide channel. In the present study additional experimental data were used to determine velocity ratio v_s/u_s, energy grade line, and C_d. The range of experiments by Novak et al. [14] was extended to cover additional 63 tests, amounting to 81 tests, listed in Table 1. Ranges of main parameters are given in Table 2.

The experiments were carried out in two glass-walled 7.5 m long flumes with a minimal slope (S_0=0.05%), one 0.2 m wide, 0.5 m deep, and the other 0.5 m wide, 0.8 m deep. Plexiglass side weirs of different sizes were placed in these flumes with a rectangular main channel $B=14$ cm and $B=30$ cm wide, respectively. In the narrower channel 6 side weirs were studied, labeled L10_p7.5, L15_p7.5, L15_p10, L20_p10, L20_p12, and L25_p12 with numbers representing dimensions in cm. Three more side weirs were examined in the wider channel: L50_p12, L75_p14, and L100_p20 (again, dimensions in cm). Flow conditions were subcritical and the lateral overflow Q_s was modular in all test runs. Adjustable rectangular sharp-crested weir was used to control the tailwater level and to provide sufficient overflow depth at side weir ($h-p\geq 2$ cm) to avoid surface tension issues. In the narrower physical model, both inflow Q_1 and flow Q_2 remaining in the main channel downstream of the side weir were measured using thin-plate V-notch weirs. Side overflow Q_s was not measured, because it spilled directly into water tank below the flume, and was calculated as Q_1-Q_2. In test runs with $B=30$ cm the Q_s spilled into a 19 cm wide parallel lateral channel. For these tests, both Q_s and Q_2 were measured using rectangular thin-plate weirs in accordance with ISO standard 1438:2008 [16] and its technical corrigendum [17], while the inflow Q_1 was measured with a larger V-notch weir. The uncertainty of flow measurements $u_c*(Q)$ was calculated using the above standard and it amounted to $u_c*(Q)=2\%$. Cross sections at $x/L=0.5$ for both sets of experiments are given in Fig. 2.

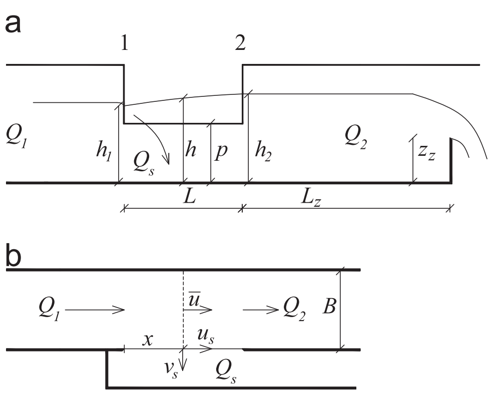

Fig. 1. Definition sketch of subcritical flow over rectangular side weir: (a) longitudinal section, (b) plan.

In Table 1, notation of test runs in the narrower flume indicates a selected basic combination of Q_1 and z_z (notation "var 0"), and whether the Q_1 was varied at fixed position z_z (variants "Q−" to "Q+" with − or + meaning lower or greater inflow), or position z_z was varied at fixed Q_1 (variants "Z−" to "Z+" with − or + meaning smaller or greater height z_z). Notation "*" indicates intermediate combinations. Distance L_z varied from $L_z=120-L$ [cm] for cases with $B=14$ cm, and $L_z=185-L$ [cm] for cases with $B=30$ cm.

Flow depths in both flumes were measured at various locations using point-gauge with 0.1 mm precision. Flow depth h_a was measured at the main channel centerline 25 cm upstream of each side weir to provide measurement in the upstream section where the water surface was parallel to the main channel bed. For tests in the narrower flume additional measurements with non-contact visualization technique were performed to determine longitudinal profiles of water surface along the side weir. A green laser (100 mW, 530–532 nm) was used to illuminate a thin vertical layer of the flow. With the flume obscured, the photos of different sections parallel to the main channel centerline were taken from perpendicularly positioned digital camera. Acquired photos were examined with the Matlab to determine grayscale values of pixels. Resulting water surface profile was calculated as a line of pixels separating a green and a black part of each photo.

Velocity fields were determined for tests in the narrower flume only, using recordings of electrolysis-generated hydrogen bubbles, as described by Novak et al. [14]. An attempt was made to use this technique in $B=30$ cm flume as well, but it turned out a more powerful DC source would be needed to produce an adequate layer of hydrogen bubbles. The principles of both visualization techniques used for test runs in the narrow flume are compared in Fig. 3.

Calibration tests were performed as described in Novak et al. [14] to achieve good agreement between measured surface velocity components and observed floats. The uncertainty of average velocity measurements $u_c*(\bar{u})$ was $u_c*(\bar{u})=2\%$.

Table 1
Main test parameters.

var.	**B=14, L=10, p=7.5 [cm]**			**B=14, L=15, p=7.5 [cm]**			**B=14, L=15, p=10 [cm]**		
	z_z[cm]	Q_1[l/s]	Q_s[l/s]	z_z[cm]	Q_1[l/s]	Q_s[l/s]	z_z[cm]	Q_1[l/s]	Q_s[l/s]
var 0	5.29	3.97	0.84	5.28	4.52	1.24	6.91	5.45	1.09
Q−	5.29	3.31	0.84	5.28	3.82	1.09	6.90	4.54	0.89
Q−*	5.29	3.68	0.88	5.28	4.19	1.14	6.90	4.99	0.96
Q+*	5.30	4.38	0.85	5.28	4.94	1.32	6.90	5.73	1.22
Q+	5.30	4.71	0.92	5.28	5.30	1.34	6.90	6.06	1.29
Z−	4.22	3.97	0.46	4.21	4.50	0.63	6.00	5.42	0.78
Z−*	4.83	3.95	0.65	4.90	4.49	0.95	6.36	5.45	0.89
Z+*	5.71	3.95	1.02	6.20	4.50	1.65	7.37	5.45	1.32
Z+	6.12	3.96	1.22	6.57	4.50	1.87	8.10	5.46	1.65
var.	**B=14, L=20, p=10 [cm]**			**B=14, L=20, p=12 [cm]**			**B=14, L=25, p=12 [cm]**		
	z_z[cm]	Q_1[l/s]	Q_s[l/s]	z_z[cm]	Q_1[l/s]	Q_s[l/s]	z_z[cm]	Q_1[l/s]	Q_s[l/s]
var 0	6.41	6.01	1.29	8.10	6.62	1.35	7.33	6.94	1.36
Q−	6.41	5.29	1.05	8.10	5.45	0.83	7.33	6.34	1.09
Q−*	6.41	5.69	1.14	8.10	6.14	1.10	7.33	6.59	1.21
Q+*	6.41	6.34	1.39	8.10	7.07	1.51	7.33	7.45	1.61
Q+	6.41	6.62	1.52	8.10	7.59	1.83	7.33	7.83	1.79
Z−	5.80	6.02	0.98	7.19	6.68	1.06	6.78	6.94	1.07
Z−*	6.11	6.02	1.14	7.78	6.64	1.19	7.70	6.91	1.52
Z+*	6.81	6.03	1.50	8.37	6.66	1.63	8.28	6.96	1.82
Z+	7.15	6.01	1.64	8.83	6.61	1.85	8.76	6.94	2.07
var.	**B=30, L=50, p=12 [cm]**			**B=30, L=75, p=14 [cm]**			**B=30, L=100, p=20 [cm]**		
	z_z[cm]	Q_1[l/s]	Q_s[l/s]	z_z[cm]	Q_1[l/s]	Q_s[l/s]	z_z[cm]	Q_1[l/s]	Q_s[l/s]
1	6.95	20.00	6.04	8.15	27.90	10.01	12.80	34.60	14.82
2	10.21	19.85	9.99	10.87	27.90	14.30	13.63	34.60	16.23
3	13.57	18.75	13.49	12.73	27.90	16.96	15.79	34.55	19.38
4	8.49	17.10	6.67	10.02	25.00	11.49	13.73	30.20	13.43
5	10.14	17.20	8.68	12.85	25.20	15.89	14.21	30.20	14.57
6	11.58	17.10	10.19	15.19	25.18	19.01	15.12	30.20	15.29
7	8.70	14.25	5.46	10.12	22.00	9.95	16.81	25.30	15.41
8	10.08	14.25	7.03	13.00	22.20	14.14	17.85	25.30	16.66
9	11.68	14.05	8.45	14.88	22.10	16.35	19.10	25.20	18.39

Table 2
Ranges of measured parameters.

Authors	B [cm]	L [cm]	p [cm]	S_0 [%]	Q_1 [l/s]	B/L [-]	Fr_1 [−]	Q_s/Q_1 [−]
Novak et al. [14]	14	10–25	7.5–12	0.05	4–7.8	0.56–1.4	0.28–0.34	0.20–0.27
Present study	14, 30	10–100	7.5–20	0.05	3.31–34.6	0.3–1.4	0.23–0.41	0.12–0.76

3. Results and discussion

3.1. Velocity ratio $u_s/\bar{u}$ and velocity distribution coefficients α and β

Our previous work (Novak et al. [14]) discussed $u_s/\bar{u}$, α, and β for variants labeled var0, Q−, and Q+ for all 6 side weirs in $B=14$ cm channel, amounting to 18 test (Table 1). In the present study, velocity fields were measured for additional 12 test runs, covering variants Z− and Z+ for all 6 side weirs in $B=14$ cm channel (Table 1). Results from these 12 runs were in accordance with conclusions presented by Novak et al. [14], and are given in Table 3 and Table 4.

3.2. Velocity ratio V_s/u_s

Measured velocity ratio v_s/u_s can be used to define deviation angle of flow Q_s, usually given only in terms of average velocity of the approach flow and the velocity of flow Q_s over the brink (*e.g.* Emiroglu et al. [4]). Velocity components u_s and v_s of the flow Q_s were examined for all 30 tests discussed in previous section, to take the full advantage of the non-invasive visualization method.

Values of the ratio v_s/u_s, given as a function of location x/L along the side weir, increased for all test runs, ranging from values 0.1 to 0.6, as Table 3 and Table 4 show. This increasing trend was in accordance with well established observations of side overflow deviation angle by previous authors. In our experiments measured ratios v_s/u_s for various side weirs increased quite rapidly in the first section of the side weir, *i.e.* along $x/L \le 0.25$, while v_s/u_s then changed less along the crest from $x/L=0.25$ to $x/L=1$, as Fig. 4 shows.

3.3. Energy grade line

In relation to the energy and momentum approach, mentioned in the introduction, the non-contactly measured water surface profiles h, average velocities $\bar{u}$ and velocity distribution coefficients α were used to determine energy grade line $E=h+\alpha^*\bar{u}^2/2\,g$ in various cross sections. While water surface elevation increased along the side weir, line E remained parallel to the main channel bed for all considered test runs. This indicates that only friction losses were present, as proposed by the energy approach.

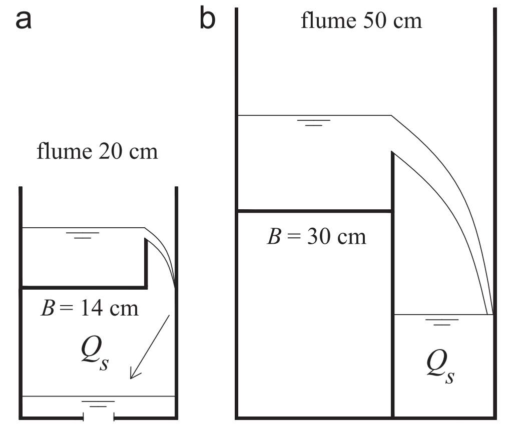

Fig. 2. Cross sections of side weirs for both sets of experiments: (a) Q_s flows into water tank, (b) Q_s is measured with a thin-plate weir in the lateral channel.

However, velocity fields were clearly non-uniform (values α from 1.01 to 1.15), as assumed by the momentum approach.

3.4. Discharge coefficient C_d

Inserting measured values from all 81 tests into C_d equations by various authors gave values C_d in the range from C_d=0.34 (using equation by Borghei et al. [7]) to C_d=0.72 (using equation by Singh et al. [5]). An even wider range of C_d from equations by various authors was reported by Emiroglu et al. [3] for L/B=3 case, which is similar to our L =100 cm, B=30 cm case. For each observed variant of our experiments, values C_d were obtained from Eq. (1) and denoted as $C_{d,mer}$ to indicate that they were calculated from measured overflows Q_s and flow depths h along the observed reach. Value h in Eq. (1) was taken as an average flow depth h_{avg} along the side weir, measured in the main channel centerline.Values $C_{d,mer}$ are shown in Table 5.

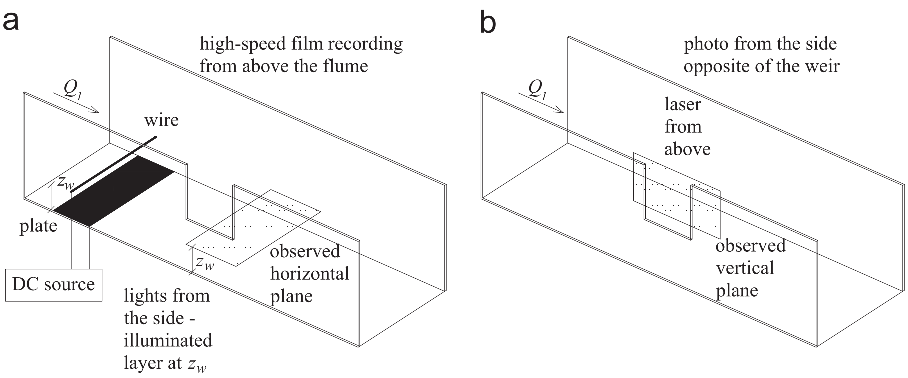

Fig. 3. Sketch of experimental set-up: (a) measurements of velocity fields using electrolysis-generated hydrogen bubbles, (b) determination of water surface longitudinal profiles using photos of laser-induced sections.

Table 3
Main results regarding velocity fields—part 1.

var	***B*=14, *L*=10, *p*=7.5 [cm]**						***B*=14, *L*=15, *p*=7.5 [cm]**						***B*=14, *L*=15, *p*=10 [cm]**					
	x/L	h/p	$\bar{u}_s/\bar{u}$	α	β	v_s/u_s	x/L	h/p	$\bar{u}_s/\bar{u}$	α	β	v_s/u_s	x/L	h/p	$\bar{u}_s/\bar{u}$	α	β	v_s/u_s
var0	0	1.33	1.03	1.02	1.01	0.32	0	1.33	0.98	1.01	1.00	0.27	0	1.26	1.08	1.02	1.01	0.16
	0.25	1.33	1.09	1.03	1.01	0.45	0.25	1.34	1.00	1.02	1.01	0.34	0.25	1.26	1.02	1.01	1.00	0.34
	0.5	1.33	1.04	1.03	1.01	0.48	0.5	1.35	1.03	1.02	1.01	0.26	0.5	1.27	1.08	1.04	1.01	0.51
	0.75	1.34	1.07	1.04	1.01	0.52	0.75	1.36	1.00	1.05	1.02	0.24	0.75	1.27	1.07	1.03	1.01	0.34
	1	1.34	1.10	1.05	1.02	0.57	1	1.37	1.02	1.04	1.01	0.35	1	1.28	1.06	1.03	1.01	0.41
Q+	0	1.38	0.98	1.02	1.01	0.30	0	1.39	1.09	1.05	1.02	0.24	0	1.28	0.94	1.01	1.00	0.39
	0.25	1.39	1.05	1.03	1.01	0.30	0.25	1.40	1.05	1.05	1.02	0.39	0.25	1.29	0.98	1.02	1.01	0.39
	0.5	1.39	1.04	1.04	1.01	0.40	0.5	1.41	1.13	1.07	1.02	0.38	0.5	1.29	1.01	1.02	1.01	0.39
	0.75	1.39	1.08	1.06	1.02	0.40	0.75	1.42	1.09	1.09	1.03	0.44	0.75	1.30	1.07	1.02	1.01	0.25
	1	1.39	1.11	1.06	1.02	0.42	1	1.43	1.20	1.13	1.04	0.40	1	1.31	1.11	1.02	1.01	0.28
Q−	0	1.27	1.00	1.03	1.01	0.31	0	1.29	1.11	1.04	1.01	0.26	0	1.21	1.00	1.01	1.00	0.32
	0.25	1.27	1.00	1.02	1.01	0.36	0.25	1.29	1.15	1.05	1.02	0.29	0.25	1.21	1.04	1.01	1.00	0.35
	0.5	1.27	0.98	1.02	1.01	0.37	0.5	1.30	1.14	1.05	1.02	0.30	0.5	1.22	1.00	1.01	1.00	0.35
	0.75	1.28	0.98	1.02	1.01	0.38	0.75	1.31	1.05	1.06	1.02	0.38	0.75	1.22	1.05	1.03	1.01	0.29
	1	1.28	1.03	1.04	1.01	0.34	1	1.31	1.03	1.05	1.02	0.37	1	1.22	0.99	1.03	1.01	0.34
Z+	0	1.40	1.18	1.08	1.03	0.34	0	1.44	1.11	1.04	1.01	0.28	0	1.33	1.06	1.03	1.01	0.35
	0.25	1.40	1.21	1.06	1.02	0.47	0.25	1.44	1.12	1.05	1.02	0.35	0.25	1.34	1.12	1.03	1.01	0.39
	0.5	1.41	1.13	1.05	1.02	0.55	0.5	1.45	1.06	1.04	1.01	0.47	0.5	1.34	1.09	1.03	1.01	0.57
	0.75	1.41	1.14	1.06	1.02	0.59	0.75	1.46	1.10	1.06	1.02	0.44	0.75	1.35	1.02	1.03	1.01	0.45
	1	1.41	1.16	1.06	1.02	0.59	1	1.47	1.07	1.04	1.01	0.34	1	1.36	1.02	1.03	1.01	0.44
Z−	0	1.22	0.94	1.02	1.01	0.18	0	1.24	1.01	1.05	1.02	0.14	0	1.20	1.05	1.04	1.01	0.27
	0.25	1.22	0.99	1.01	1.00	0.25	0.25	1.24	0.99	1.05	1.02	0.18	0.25	1.20	1.12	1.06	1.02	0.29
	0.5	1.22	0.98	1.02	1.01	0.33	0.5	1.25	1.07	1.08	1.03	0.30	0.5	1.20	1.17	1.10	1.04	0.25
	0.75	1.22	1.02	1.04	1.01	0.38	0.75	1.26	1.04	1.08	1.03	0.25	0.75	1.20	1.17	1.12	1.04	0.22
	1	1.22	1.06	1.04	1.01	0.31	1	1.26	1.09	1.08	1.03	0.25	1	1.21	1.22	1.16	1.05	0.22

Table 4
Main results regarding velocity fields—part 2.

var	B=14, L=20, p=10 [cm]						B=14, L=20, p=12 [cm]						B=14, L=25, p=12 [cm]					
	x/L	h/p	$\bar{u}_s/\bar{u}$	α	β	v_s/u_s	x/L	h/p	$\bar{u}_s/\bar{u}$	α	β	v_s/u_s	x/L	h/p	$\bar{u}_s/\bar{u}$	α	β	v_s/u_s
var0	0	1.24	1.05	1.03	1.01	0.13	0	1.19	1.00	1.03	1.01	0.31	0	1.16	0.97	1.04	1.02	0.29
	0.25	1.24	1.14	1.08	1.03	0.39	0.25	1.19	1.15	1.13	1.04	0.45	0.25	1.17	1.10	1.08	1.03	0.32
	0.5	1.25	1.06	1.02	1.01	0.33	0.5	1.20	1.04	1.03	1.01	0.42	0.5	1.17	1.04	1.04	1.01	0.29
	0.75	1.25	1.08	1.02	1.01	0.33	0.75	1.20	1.10	1.08	1.03	0.47	0.75	1.18	1.17	1.17	1.06	0.33
	1	1.26	1.19	1.05	1.02	0.37	1	1.20	1.04	1.05	1.02	0.49	1	1.18	1.14	1.09	1.03	0.35
Q+	0	1.26	1.01	1.04	1.01	0.31	0	1.22	1.13	1.07	1.02	0.30	0	1.19	1.10	1.06	1.02	0.23
	0.25	1.27	1.09	1.07	1.02	0.37	0.25	1.23	1.20	1.09	1.03	0.41	0.25	1.20	1.13	1.08	1.03	0.36
	0.5	1.27	1.06	1.02	1.01	0.38	0.5	1.23	1.15	1.07	1.02	0.42	0.5	1.21	1.11	1.04	1.01	0.29
	0.75	1.28	1.11	1.05	1.02	0.38	0.75	1.24	1.20	1.09	1.03	0.45	0.75	1.21	1.17	1.07	1.03	0.33
	1	1.29	1.13	1.04	1.01	0.44	1	1.24	1.24	1.08	1.03	0.50	1	1.22	1.15	1.06	1.02	0.36
Q−	0	1.20	1.07	1.04	1.01	0.15	0	1.14	1.03	1.03	1.01	0.37	0	1.14	1.11	1.05	1.02	0.18
	0.25	1.20	1.08	1.03	1.01	0.35	0.25	1.15	1.12	1.04	1.01	0.41	0.25	1.15	1.14	1.06	1.02	0.21
	0.5	1.21	1.06	1.02	1.01	0.30	0.5	1.15	1.08	1.02	1.01	0.35	0.5	1.16	1.10	1.04	1.01	0.24
	0.75	1.21	1.11	1.05	1.02	0.36	0.75	1.15	1.09	1.04	1.01	0.39	0.75	1.16	1.21	1.06	1.02	0.28
	1	1.22	1.13	1.05	1.02	0.41	1	1.16	1.11	1.04	1.01	0.35	1	1.16	1.25	1.05	1.02	0.22
Z+	0	1.27	1.06	1.03	1.01	0.23	0	1.24	1.12	1.06	1.02	0.22	0	1.22	1.15	1.11	1.04	0.15
	0.25	1.28	1.07	1.06	1.02	0.42	0.25	1.24	1.21	1.07	1.02	0.43	0.25	1.23	1.18	1.12	1.04	0.37
	0.5	1.29	1.03	1.03	1.01	0.43	0.5	1.25	1.05	1.04	1.01	0.47	0.5	1.23	1.12	1.06	1.02	0.32
	0.75	1.30	1.07	1.04	1.02	0.37	0.75	1.26	1.09	1.04	1.02	0.53	0.75	1.24	1.21	1.12	1.04	0.40
	1	1.31	1.07	1.02	1.01	0.40	1	1.27	1.09	1.06	1.02	0.49	1	1.24	1.24	1.08	1.03	0.43
Z-	0	1.20	1.07	1.02	1.01	0.18	0	1.16	1.03	1.04	1.01	0.30	0	1.14	1.07	1.08	1.03	0.17
	0.25	1.20	1.11	1.05	1.02	0.29	0.25	1.17	1.11	1.06	1.02	0.32	0.25	1.15	1.13	1.05	1.02	0.23
	0.5	1.21	1.06	1.02	1.01	0.29	0.5	1.18	1.08	1.03	1.01	0.30	0.5	1.15	1.15	1.06	1.02	0.21
	0.75	1.22	1.17	1.08	1.03	0.34	0.75	1.18	1.19	1.06	1.02	0.32	0.75	1.15	1.22	1.12	1.04	0.20
	1	1.23	1.30	1.10	1.03	0.36	1	1.19	1.24	1.03	1.01	0.37	1	1.16	1.29	1.08	1.03	0.27

In Table 5, notation of test runs in the wider flume gives information about inflow in l/s and spilling ratio Q_s/Q_1, with notation "a" representing the smallest ratio (around $Q_s/Q_1=0.3$ to 0.4) and notation "c" indicating the greatest ratio (around $Q_s/Q_1=0.6$ to 0.7). Exceedingly high values of $C_{d,mer}$ and high standard deviation values (STDEV) for the smallest two side weirs (L10_p7.5 and L15_p7.5 in Table 5) suggested that some flow measurements for these two configurations were probably not reliable enough. For this reason, results from L10_p7.5 and L15_p7.5 side weirs were not used for the formulation of C_d equation. Consequently, the range of validity of C_d equation was adjusted. With the elimination of results from the smallest two observed side weirs, 63 results remained, and the experimental limits were the following: $B=14$ to 30 cm, $L=15$ to 100 cm, $p=10$ to 20 cm, $Q_1=4.54$ to 34.6 l/s, $Q_s=0.89$ to 19.38 l/s, and $Fr_1=0.23$ to 0.41.

Dimensional analysis was used to formulate an equation for C_d on the basis of our experimental data. In doing so, various dimensionless ratios were considered. Finally, the following power-law term was found to be the most suitable:

$$C_{d,mer} = KFr_1^{\delta}(h_2/p)^{\varepsilon}(B/L)^{\zeta} \quad (2)$$

with unknown constant K, and unknown exponents δ, ε, and ζ. Eq. (2) formed a system of equations when the measured quantities were inserted. A logarithm (ln) operation was used to obtain a system of linear equations for unknown variables. This system was solved in Matlab to determine the mentioned unknowns and resulting values C_d. From all the data from test runs L15_p10 to L100_p20, the following equation was obtained:

$$C_d = 0.4689Fr_1^{-0.166}(h_2/p)^{-0.047}(B/L)^{-0.135} \quad (3)$$

The correlation between $C_{d,mer}$ and C_d from Eq. (3) was observed in terms of correlation coefficient r. To achieve $r=0.85$ value, only additional 2 out of 63 considered experimental results had to be eliminated.

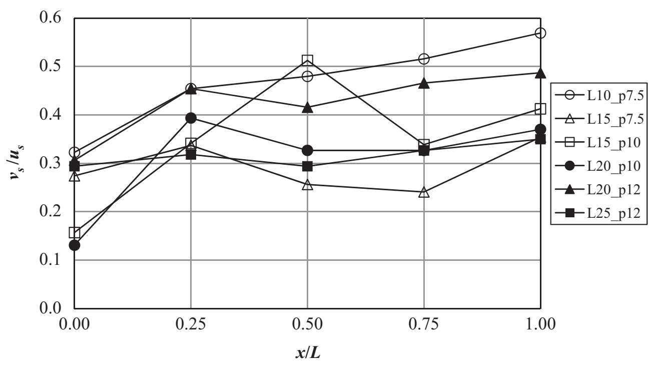

Fig. 4. Values v_s/u_s for observed side weirs in narrow flume (B=14 cm)—variants labeled var0 only.

The Eq. (3) is suitable for practical applications, as it includes Fr_1 (in accordance with the great majority of equations by other authors), ratio h_2/p (*e.g.* like May et al. [13]), and B/L (*e.g.* like Borghei et al. [7], and Emiroglu et al. [4]). For the investigated side weirs L15_p10 to L100_p20, the Eq. (3) gives C_d values which are similar to ones calculated from the following equations:

$$C_d = 0.650 - 0.149\,[(h_2-p)/p]^{0.0868}[L/(h_2-p)]^{-0.303}(h_2/p)^{0.149}$$

by May et al. [13] and

$$C_d = 0{,}81 - 0{,}6Fr_1$$

by Ranga Raju et al. [18].

When our experimental data was inserted in the following equations:

$$C_d = 0{,}33 - 0{,}18Fr_1 + 0{,}49\,(p/h_1)$$

Table 5
Values $C_{d,mer}$ for all measured cases.

variant	Narrower flume (B=14 cm)						Wider flume (B=30 cm)					
	L10_p7.5	L15_p7.5	L15_p10	L20_p10	L20_p12	L25_p12	var.	L50_p12	var.	L75_p14	var.	L100_p20
var0	0.72	0.66	0.56	0.56	0.63	0.61	20_a	0.65	28_a	0.63	35_a	0.67
Q−	0.97	0.73	0.63	0.59	0.59	0.59	20_b	0.63	28_b	0.61	35_b	0.66
Q−*	0.86	0.67	0.58	0.55	0.58	0.60	20_c	0.58	28_c	0.61	35_c	0.63
Q+*	0.63	0.65	0.59	0.56	0.61	0.61	17_a	0.62	25_a	0.63	30_a	0.69
Q+	0.63	0.56	0.57	0.57	0.66	0.63	17_b	0.63	25_b	0.63	30_b	0.70
Z−	0.74	0.56	0.61	0.54	0.59	0.60	17_c	0.62	25_c	0.62	30_c	0.66
Z−*	0.72	0.60	0.56	0.56	0.62	0.62	14_a	0.66	22_a	0.64	25_a	0.71
Z+*	0.75	0.65	0.59	0.57	0.60	0.61	14_b	0.64	22_b	0.63	25_b	0.69
Z+	0.77	0.68	0.59	0.57	0.60	0.61	14_c	0.64	22_c	0.63	25_c	0.68
AVG	0.76	0.64	0.59	0.56	0.61	0.61		0.63		0.63		0.68
STDEV	0.107	0.057	0.022	0.014	0.026	0.011		0.022		0.009		0.024

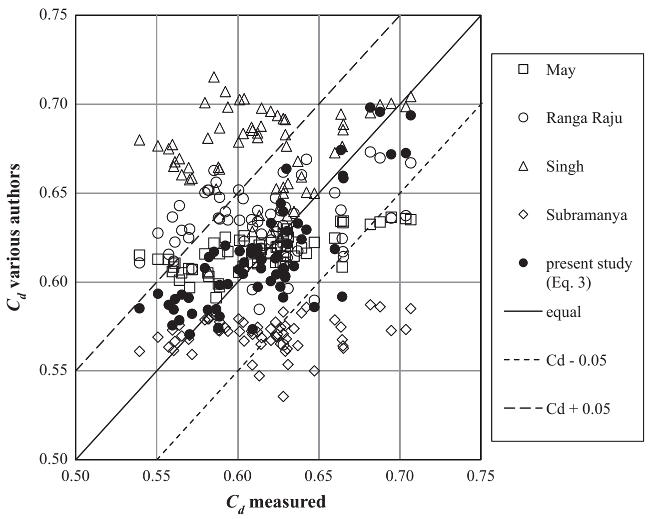

Fig. 5. C_d measured (*i.e.* calculated from Eq. (1)) *versus* C_d by various authors, for 63 experimental data from L15_p10 to L100_p20 side weirs.

by Singh et al. [5] and

$$C_d = 0{,}864\,[(1-Fr_1^2)/(2+Fr_1^2)]^{0.5}$$

by Subramanya and Awasthy [19], the considerable number of calculated C_d values fell out of the $\pm$0.05 region (dashed lines in Fig. 5). For the same experimental data the equations by authors, other than those shown in Fig. 5, gave values C_d that deviated considerably from C_d of Eq. (3).

4. Conclusions

Our previous work concerning subcritical flow at sharp-crested rectangular side weirs in rectangular straight channels was extended to cover a wider range of measured geometrical and hydraulic parameters. Both longitudinal water surface profiles and velocity fields at horizontal planes were determined using non-invasive visualization techniques, *i.e.* photos of laser-induced sections and films of electrolysis-generated hydrogen bubbles.

The present study confirmed velocity fields at side weir were clearly non-uniform with velocity ratios $u_s/\bar{u}$ and v_s/u_s increasing along the side weir from 1 to 1.2 and 0.1 to 0.6, respectively, and kinetic energy correction coefficient α ranging from 1.01 to 1.15 along the side weir. However, the energy grade line, calculated from the measured flow depths and velocities, remained parallel to the main channel bed for all considered test runs.

New phenomenological equation for the discharge coefficient C_d of the rectangular sharp-crested side weir in narrow flume was developed using dimensional analysis from experimental data covering the following range of parameters: B=14 and 30 cm, L=15 to 100 cm, p=10 to 20 cm, Q_1=4.54 to 34.6 l/s, Q_s=0.89 to 19.38 l/s and Fr_1=0.23 to 0.41.The proposed equation gives C_d values which are in good agreement with two other studies in literature.

Acknowledgments

The authors acknowledge the financial support of the Slovenian Research Agency (ARRS) in the project Development of a computer-aided visualization method for the diagnostics of velocity fields in hydrodynamic systems.

References

[1] Rosier B. Interaction of side weir overflow with bed-load transport and bed morphology in a channel. Lausanne: Ecole Polytechnique Federale De Lausanne; 2007.
[2] De Marchi G. Essay on the performance of lateral weirs. L'Energia Electtrica, Milan 1934;11(11):849–60 in Italian.
[3] Hager WH. Wastewater hydraulics: Theory and practice. 2nd ed. Berlin: Springer; 2010.
[4] Emiroglu ME, Agaccioglu H, Kaya N. Discharging capacity of rectangular side weirs in straight open channels. Flow Measurement and Instrumentation 2011;22:319–30.
[5] Singh R, Manivannan D, Satyanarayana T. Discharge coefficient of rectangular side weirs. Journal of Irrigation and Drainage Engineering 1994;120:814–9.
[6] Swamee PK, Pathak SK, Mohan M, Agrawal SK, Ali MS. Subcritical flow over rectangular side weir. Journal of Irrigation and Drainage Engineering 1994;120:212–7.
[7] Borghei SM, Jalili MR, Ghodsian M. Discharge coefficient for sharp-crested side weir in subcritical flow. Journal of Hydraulic Engineering 1999;125:1051–6.
[8] Yüksel E. Effect of specific energy variation on lateral overflows. Flow Measurement and Instrumentation 2004;15:259–69.
[9] Venutelli M. Method of solution of non-uniform flow with the presence of rectangular side weir. Journal of Irrigation and Drainage Engineering 2008;134:840–6.
[10] El-Khashab A, Smith KVH. Experimental investigation of flow over side weirs. Journal of Hydraulic Division ASCE 1976;102:1255–68.
[11] Hager WH, Volkart PU. Distribution channels. Journal of Hydraulic Engineering 1986;112:935–52.
[12] Lee K-L, Holley ER. Physical modeling for side-channel weirs. CRWR Online Report 02-2. 2002; 〈http://www.crwr.utexas.edu/reports/pdf/2002/rpt02-02.pdf〉 (accessed 08.03.2011).
[13] May RWP, Bromwich BC, Gasowski Y, Rickard CE. Hydraulic design of side weirs. London: Thomas Telford; 2003.

[14] Novak G, Steinman F, Müller M, Bajcar T. Study of velocity field at model sideweir using visualization method. Journal of Hydro-environment Research 2012;50:129–33.

[15] Bajcar T, Širok B, Eberlinc M. Quantification of flow kinematics using computer-aided visualization. Journal of Mechanical Engineering 2009;55:215–23.

[16] International standard ISO 1438:2008(E). Hydrometry–Open channel flow measurement using thin-plate weirs. Switzerland: International Organization for Standardization; 2008.

[17] International standard ISO 1438:2008—Technical Corrigendum 1. Hydrometry–Open channel flow measurement using thin-plate weirs Switzerland: International Organization for Standardization; 2008.

[18] Ranga Raju KG, Prasad B, Grupta SK. Side weir in rectangular channel. ASCE Journal of the Hydraulics Division 1979;105(5):547–54.

[19] Subramanya K, Awasthy SC. Spatially varied flow over side weirs. ASCE Journal of the Hydraulics Division 1972;98(1):1–10.